Journal of Membrane Science 679 (2023) 121697

Contents lists available at ScienceDirect

Journal of Membrane Science

journal homepage: www.elsevier.com/locate/memsci

CO_2 separation using thin film composite membranes of acid-hydrolyzed PIM-1

Ming Yu [a,b], Andrew B. Foster [b], Mustafa Alshurafa [b], Jose Miguel Luque-Alled [c,d], Patricia Gorgojo [c,d], Sandra E. Kentish [a], Colin A. Scholes [a,**], Peter M. Budd [b,*]

[a] Department of Chemical Engineering, The University of Melbourne, Melbourne, VIC, 3010, Australia
[b] Department of Chemistry, School of Natural Sciences, The University of Manchester, Manchester, M13 9PL, UK
[c] Departamento de Ingeniería Química y Tecnologías del Medio Ambiente, Universidad de Zaragoza, C/ Pedro Cerbuna 12, 50009, Zaragoza, Spain
[d] Instituto de Nanociencia y Materiales de Aragón (INMA) CSIC-Universidad de Zaragoza, C/ Mariano Esquillor s/n, 50018, Zaragoza, Spain

ARTICLE INFO

Keywords:
PIM-1
Acid hydrolysis
Polymer microstructure
Thin film composite
Membrane aging
Plasticization
CO_2 gas separation

ABSTRACT

The polymer of intrinsic microporosity PIM-1 was synthesized with different topologies and negligible network content. A more rapid heating rate from room temperature yielded a predominantly di-substituted PIM-1 (D-PIM-1), whereas a marginally lower heating rate produced a more branched structure (B-PIM-1). Both polymers were acid-hydrolyzed to give carboxylic acid functionalization (cPIM-1), as indicated by FT-IR, ^{1}H NMR, and elemental analysis. Both PIM-1 and cPIM-1 were processed into self-supported membranes and into thin film composite (TFC) membranes on a polyacrylonitrile support. For a 70% hydrolyzed polymer (D-cPIM-1-70%), the initial CO_2 permeance reached 7700 GPU, with ideal selectivity of 56 for CO_2/N_2 and 37 for CO_2/CH_4. D-PIM-1 and D-cPIM-1-70% showed 85% and 52% CO_2 permeance drop after 60 days' aging, respectively. B-PIM-1, with initial CO_2 permeance of 3100 GPU and ideal selectivity of 19 for CO_2/N_2 and 11 for CO_2/CH_4, showed only a 65% decrease. Polymer that was both branched and hydrolyzed (B-cPIM-1-73&81%), with CO_2 permeance of 3200 GPU and selectivity of 64 for CO_2/N_2 and 45 for CO_2/CH_4, showed no decrease of CO_2 permeance after 60 days. The branched structure is crucial for reducing membrane aging. Plasticization gave rise to reduced selectivity in mixed gas experiments, but nevertheless TFC membranes prepared from B-cPIM-1-81% were able to concentrate CO_2 to 38% from a 10% CO_2/90% N_2 mixture at 4.8 bar.

1. Introduction

Excessive CO_2 emission to the atmosphere caused by anthropogenic activities such as fossil fuel combustion has led to global warming [1–3]. Membranes are promising tools for carbon capture due to the advantages of module compactness, operational simplicity, energy efficiency and easy scalability [4,5]. Various types of polymer membranes [6–13] have been developed, many exhibiting highly CO_2 permeable and selective properties over competing gases such as N_2 and CH_4, but all these membranes are hampered by the permeability-selectivity trade-off [14,15].

Most studies of novel membrane materials are characterized through the performance of relatively thick films, with thicknesses of tens to hundreds of micrometres. Thin film composite (TFC) membranes with active layer thicknesses less than a couple of micrometres are more attractive for industrial applications [4,16,17]. Defect-free and thin selective layers can maximize gas throughput by minimizing transmembrane resistance, without sacrificing gas selectivity, to meet industrial requirements. Merkel et al. [18] suggested an optimum region for industrial post-combustion CO_2 capture using such TFC membranes of CO_2 permeance more than 1000 GPU and CO_2/N_2 selectivity in the range of 20–150.

Recent studies have focused on developing ultra-thin TFC membranes with active layer thickness ranging from 50 to 300 nm. To achieve this target, complex systems often have to be adopted, such as a mixed-matrix active layer [19–22], additional (modified) gutter layer [23,24], surface polymerization [25,26] and development of new materials [27,28]. Lee et al. [22] successfully fabricated mixed-matrix TFC membranes of poly(vinyl imidazole)-poly(oxyethylene methacrylate) copolymer with ZIF-8. A 300 nm active layer containing 50% ZIF gave

* Corresponding author.
** Corresponding author.
E-mail addresses: cascho@unimelb.edu.au (C.A. Scholes), peter.budd@manchester.ac.uk (P.M. Budd).

https://doi.org/10.1016/j.memsci.2023.121697
Received 6 August 2022; Received in revised form 6 April 2023; Accepted 25 April 2023
Available online 26 April 2023

CO_2 permeance of 4474 GPU and CO_2/N_2 selectivity of 32. Fu et al. [25] developed a surface polymerization method to graft a 100 nm dense selective layer directly on top of a modified support and the TFC membrane showed a CO_2 permeance of 1260 GPU and CO_2/N_2 selectivity of 43. Qiao et al. [29] prepared a thinner metal-induced, ordered microporous polymer layer of less than 50 nm and showed 3000 GPU for CO_2 with CO_2/N_2 selectivity of 78.

Polymers of intrinsic microporosity (PIMs), first reported by Budd and McKeown in 2004 [6], have received much attention due to their highly contorted polymer structure and inefficient packing, which provides high free volume and high gas permeability [30]. The excellent solubility in chloroform and tetrahydrofuran endows the original PIM-1 with good processibility. By controlling the polymerization conditions, such as the temperature profile, purging nitrogen flow and monomer reactivity, PIM-1 samples with different topologies, including branched and network structures, can be synthesized [31–33]. These structurally different variants of PIM-1 show differences in membrane performance, especially in terms of aging [34]. Furthermore, the nitrile group of PIM-1 allows further chemical modification such as amination [35], amidoximation [36,37], carboxylation [38–40] and chemical cross-linking [41].

The base hydrolysis method has been much developed over the years and was originally believed to yield a carboxylated-PIM-1. However, this early method was later found mainly to produce an amide group, rather than carboxylic acid [38,42]. Base hydrolyzed PIM-1 membranes exhibit improved separation performance [43,44] and can also incorporate metal ions [45–48]. Methods have been developed to give a high –COOH conversion by long-term base hydrolysis [39], nitrous acid post treatment of amide-PIM-1 [49,50], and acid hydrolysis [40,51] methods. The intense hydrogen bonding interaction caused by a carboxylic acid rich environment provides a better molecular sieving effect for CO_2 separation [40], but the densely packed structure also results in reduced free volume and gas permeability. Jeon et al. [39] synthesized PIM-COOH using a 360 h base hydrolysis method with more than 92% conversion, and the carboxylation resulted in thick films exhibiting an initial CO_2 permeability decrease from 3934 barrer to 96 barrer, with CO_2/N_2 selectivity increase from 14.6 to 52.6. Rodriguez et al. [40] developed a more time-efficient 2-day acid hydrolysis method to synthesize PIM-COOH with 96% conversion, and this functionalization resulted in a CO_2 permeability decrease from 2800 barrer to 290 barrer with an increase in CO_2/N_2 selectivity from 20 to 32.

In the present work, we prepared highly permeable and selective TFC membranes on a polyacrylonitrile (PAN) support using acid-hydrolyzed, carboxylated PIM-1 through an industrially applicable kiss-coating method. Two variants of PIM-1 were investigated, one predominantly di-substituted (D-PIM-1) and the other more branched (B-PIM-1). The TFC membranes were coated from polymer solutions in tetrahydrofuran (THF), which is generally a challenging solvent for a PAN support. However, thin active layers with thickness ranging from 600 nm to 3.4 μm were directly coated onto the support without any gutter layer. Some TFC membranes exhibited evidence of penetration into the bulk of the PAN support, which does not adversely affect membrane performance. Membranes were characterized by single gas permeation of N_2, CH_4 and CO_2. To the best of our knowledge, ideal gas separation performance of the branched and hydrolyzed PIM-1 TFC membrane, B-cPIM-1-73&81%, is beyond any other reported PIM-1 based TFC membranes. However, plasticization may occur under the conditions of use, as indicated by studies of the pressure dependence of CO_2 permeability, and by mixed gas testing (10% CO_2, 90% N_2).

2. Experimental section

2.1. Materials

5,5',6,6'-Tetrahydroxy-3,3,3',3'-tetramethyl-1,1'-spirobisindane (TTSBI, 97%) was purchased from Alfa Aesar. Tetrafluoroterephthalonitrile (TFTPN, >99%) was purchased from Fluorochem. Potassium carbonate (K_2CO_3, anhydrous, ≥99.5%), tetrahydrofuran (THF, analytical reagent grade, ≥99.8%), sulfuric acid (H_2SO_4, laboratory reagent grade, ≥95%) and glacial acetic acid (analytical reagent grade, ≥99.7%) were purchased from Fisher Scientific. Toluene (ACS reagent, ≥99.7%), N,N-dimethylacetamide (DMAc, anhydrous, 99.8%), chloroform (HPLC, ≥99.8%), methanol (ACS reagent, ≥99.8%), 1,4-dioxane (anhydrous, 99.8%), acetone (for analysis), ethyl acetate (GC, ≥99.5%), hexane (HPLC, ≥97%), chloroform-d (99.8 atom %D) and glass wool were purchased from Sigma-Aldrich. Dimethylsulfoxide-d_6 (DMSO-d_6, D, 99.9%) was purchased from Cambridge Isotope Laboratories, Inc. Sepro PA350 polyacrylonitrile (PAN) ultrafiltration membrane support was kindly supplied by Prof. Ingo Pinnau, KAUST. UF010104 PAN support (batch G) was purchased from SolSep BV (The Netherlands).

The TTSBI monomer required further purification prior to use. 40 g TTSBI was first refluxed in 667 ml ethyl acetate at 90 °C for 2 h, then 667 ml hexane was added. The contents were left refluxing for 10 further minutes, before being cooled down in ice for 3 h. Purified TTSBI was recovered by filtration and dried under vacuum for at least 1 day before use.

2.2. PIM-1 synthesis, purification and characterization

PIM-1 was synthesized based on the high temperature method [52] but modified into a larger scale with a different solvent addition process. 17.03 g (50 mmol) TTSBI, 9.99 g (50 mmol) TFTPN and 20.73 g (150 mmol) K_2CO_3 were added into a 500 ml three-neck round-bottom flask placed in a heating block (Asynt, UK) on top of a RCT basic hot plate magnetic stirrer (IKA, UK) which was set at 160 °C. Heating block temperature was monitored by a temperature sensor. The flask was fitted with a N_2 purge inlet, an open-end coil condenser, and an overhead stirrer (Hei-TORQUE Expert 100, Germany). Solvent was prepared by mixing DMAc and toluene at a ratio of 2:1. The system was pre-purged by N_2 flow. 180 ml (20% excess on the 150 ml normally used) solvent mixture was added into the flask [33]. The overhead stirrer with initial speed of 250 rpm and hot plate were turned on immediately, accompanied with a strong positive N_2 flow. The stir speed was increased appropriately over the time of the reaction, based on the increasing viscosity. The extra solvent present at the start changes the temperature profile of the reaction mixtures at the very start compared to a conventional PIM-1 polymerization. In addition, different approaches to heating the reaction mixture were employed to further examine the role of this temperature profile. For di-substituted PIM-1 (D-PIM-1) synthesis, a small heating block (dish) was used to give a rapid heating rate, initially at 13.9 °C min^{-1}. Two batches of 30 ml solvent mixture were added at 11 min and 18 min, respectively, and the reaction was stopped at 30 min, with an average temperature of 141 °C over the reaction period. For branched PIM-1 (B-PIM-1), a larger heating block was used to give a slower heating rate, initially at 10.5 °C min^{-1}. Two batches of 30 ml solvent mixture were added at 15 min and 22 min, and the reaction was stopped at 40 min, with an average temperature of 127 °C. The temperature, stir speed and torque profile can be seen in Fig. S1. The reaction scheme is shown in Fig. 1 [31,34].

Each reaction was quenched with excess methanol. The precipitated PIM-1 polymer was collected by vacuum filtration and re-dissolved in 550 ml chloroform in the case of D-PIM-1 and 700 ml for B-PIM-1 (structurally different polymers solubilize differently in chloroform). After the polymer was totally dissolved, PIM-1 was reprecipitated by slowly pouring the solution into excess methanol. The PIM-1 recovered after vacuum filtration was refluxed in de-ionized water overnight and then vacuum filtered again. PIM-1 was immersed in a minimum amount of 1,4-dioxane (just enough to cover the polymer) for 15 min and then washed by copious amounts of acetone and methanol, followed by immersing in methanol overnight. Finally, vacuum collected PIM-1 was dried at 100 °C in an oven for 1 day and at 120 °C in a vacuum oven for

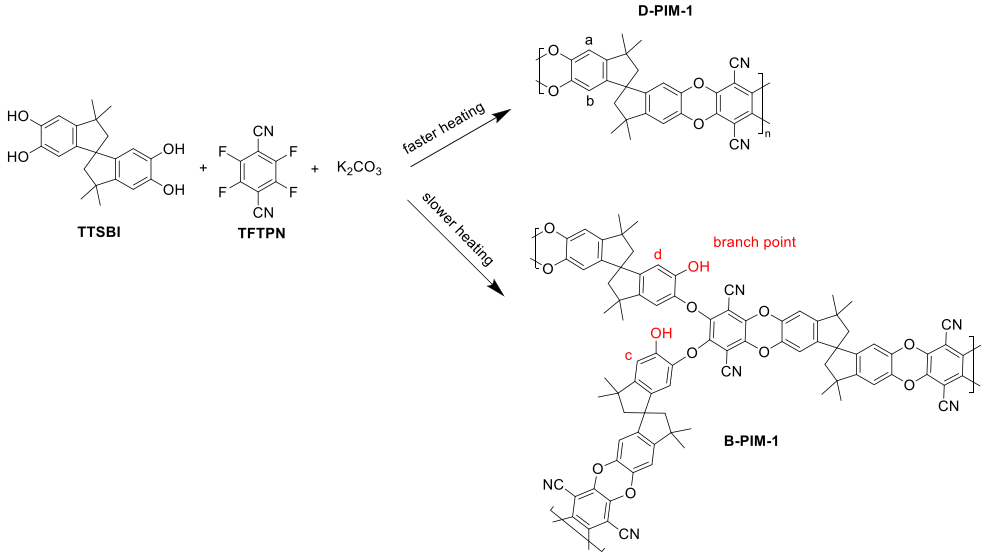

Fig. 1. Step growth polymerizations of TTSBI and TFTPN to produce D-PIM-1 and B-PIM-1.

another two days to remove any remaining solvent.

Proton nuclear magnetic resonance (^{1}H NMR) spectra were recorded from 25 mg ml^{-1} solutions of PIM-1 in deuterated chloroform using a Bruker Avance II 500 MHz instrument. Lorentz peak fitting of the aromatic proton region ($\delta = 6.0-7.2$ ppm) of each proton NMR spectrum was used to determine the respective integral areas associated with resonances attributed to di-substituted PIM-1 residue and branch point stuctures (aromatic protons labeled **a**, **b**, **c** and **d** in Fig. 1). The peak fittings obtained for the aromatic proton regions of ^{1}H NMR spectra of D-PIM-1 and B-PIM-1 (Figs. S2 and S3) polymers are presented in Figs. S4 and S5. This allowed an estimation of the percentage of branch points present in each PIM polymer sample as a proportion of all residues present.

Number-average molar mass M_n, weight-average molar mass M_w, and dispersity $Đ$ of the PIM-1 polymers were determined through gel permeation chromatography (GPC). Sample solutions were prepared as 1 mg ml^{-1} polymer solutions in chloroform, which were then filtered through a polytetrafluoroethylene (PTFE) membrane filter (0.45 μm, Fisherbrand) before analysis. Samples were analyzed with a flow rate of 1 ml min^{-1} using a Viscotek VE2001 SEC solvent/sample module with two PL Mixed B columns and a Viscotek TDA 302 triple detector array (refractive index, light scattering, viscosity detectors). Data was analyzed using OmniSEC software and a 110 kg mol^{-1} polystyrene standard was used for system calibration.

Elemental analysis was performed by a Flash 2000 Organic Elemental Analyser (Thermo Scientific, The Netherlands). Ultraviolet–Visible (UV–Vis) spectroscopy was collected from 0.09 mM PIM-1 tetrahydrofuran (THF) solutions using a Varian Cary 5000 UV–Vis NIR spectrophotometer at room temperature. Fourier-transform infrared spectroscopy (FT-IR) was carried out with a Nicolet iS 5 FT-IR Spectrometer (ThermoFisher Scientific). Powder X-ray diffraction (PXRD) was performed on a Philips X'pert X-ray diffractometer (40 kV and 30 mA) using Cu-Kα radiation ($\lambda = 1.5406$ Å). The data were collected at room temperature in a 2θ range of 5–50 with a scan speed of 4° min^{-1}. Dynamic light scattering (DLS) data were collected from 50 ppm polymer solutions in THF using a Malvern Zetasizer Nano ZS instrument at room temperature. Thermogravimetric analysis (TGA) was performed by a PerkinElmer TGA DSC 8000 System. The polymer was heated up from room temperature to 150 °C at a rate of 10 °C min^{-1} under nitrogen and maintained at 150 °C for an hour to remove any moisture. Then polymers were heated up to 600 °C at 10 °C min^{-1} for thermal degradation measurements.

PIM-1 network content measurements were also performed. 10 mg of each PIM-1 sample was dissolved in 10 ml chloroform and the solution filtered through a 0.45 μm PTFE membrane filter to remove any colloidal network content. The collected filtered solution was left open in a fume hood at room temperature for evaporation of chloroform. The polymer remaining after solvent evaporation was measured by weight. Network content was calculated based on the following equation:

$$Network\ content = \frac{w - w_r}{w} \times 100\% \quad (1)$$

where w was the initial weight of PIM-1 and w_r was the weight of PIM-1 remaining after filtration [31].

2.3. PIM-1 acid hydrolysis, purification and characterization

The acid hydrolysis of PIM-1 was a scaled up version (×16) of the method described by the Smith group [40]. In short, 288 ml deionized (DI) water, 288 ml H_2SO_4, 96 ml glacial acetic acid and 4.8 g PIM-1 were added into a 1 L round bottom flask in sequence. The flask was fitted with a coil condenser and placed into a heating block on top of a hot plate. The reaction was conducted at 150 °C under continuous stirring for either 24 h or 48 h. The hydrolysis reaction for the di-substituted PIM-1 sample is presented in Fig. 2.

The solution was then cooled down and neutralized in 8 L de-ionized (DI) water. The precipitated carboxylated PIM-1 (cPIM-1) was vacuum filtered and refluxed overnight in slightly acidic DI water, prepared by adding 15 drops of H_2SO_4 into 2.5 L DI water. Finally, cPIM-1 was collected by vacuum filtration and dried at 120 °C in a vacuum oven for two days.

^{1}H NMR analysis of each cPIM-1 was carried out in deuterated DMSO solution (25 mg ml^{-1}). FT-IR, TGA, XRD, UV–Vis, elemental analysis were performed to quantify the success of carboxylated PIM-1 conversion, with equipment details mentioned in the previous section. Hydrolyzed PIM-1s are named as D/B-cPIM-1-X%, where D and B represent di-substituted and branched structure, respectively, and X represents the hydrolysis conversion.

2.4. Preparation of self-standing membranes

Self-standing membranes were prepared of PIM-1 and cPIM-1 by casting from 3% w/v solutions in chloroform and THF, respectively. 0.15 g polymer dissolved in 5 ml of solvent was pre-filtered through

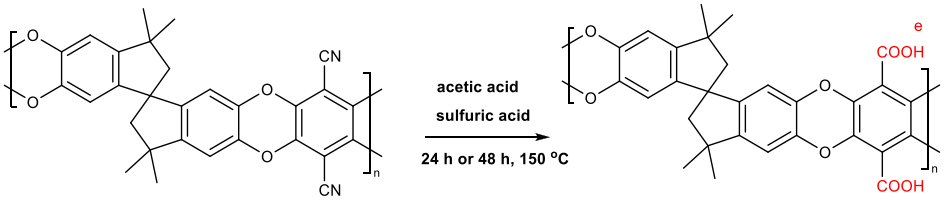

Fig. 2. Acid hydrolysis of D-PIM-1.

glass wool to remove any solid impurities or network, and each filtered solution was poured into a polytetrafluoroethylene (PTFE) Petri dish with a diameter of 60 mm. The Petri dish was loosely covered with a bigger glass Petri dish and placed in a N_2 cabinet at room temperature to allow slow solvent evaporation and film formation over 2–3 days. The films were peeled from the petri dishes and placed in a 120 °C vacuum oven overnight to remove any remaining solvent. Film thicknesses were measured six times for each membrane using a digimatic micrometer (Mitutoyo, Japan). Average thicknesses of PIM-1 films were 48 ± 3 μm and of cPIM-1 films were 40 ± 2 μm.

2.5. Preparation of thin film composite membranes

TFC membranes were prepared by a kiss coating method using a roller coater (Fig. S6). The PAN support was cut into a 4.5 cm × 10 cm rectangular sheet and applied to the roller wheel, with edges sealed with aluminum tape to prevent any solution penetration to the sheet bottom and ensure only top-side coating. The programmable DC power supply motor (RS-3005P, RS PRO, UK) was set at 15 V and the current reading at 0.14 A to ensure a total coating time of about 5 s (solution contact time in 1 revolution). Coating solutions were prepared as 3% w/v THF PIM-1 solution and 4–6% w/v THF cPIM-1 solution. In the coating process, the amount of contact between the coating solution and the support sheet on the roller wheel was controlled by tuning the number of glass slides placed under the solution tray. The solution concentration, *y*, used to cast the TFC membranes is prefixed as *y* % w/v in front of the designated polymer name. After coating, sheets were peeled off from the roller and placed in a N_2 cabinet at room temperature overnight, prior to permeance testing.

The thickness of the PIM-1 layer on the PAN support was determined by transmission electron microscopy (TEM) analysis. For the preparation of the TEM specimens, the TFC samples were embedded in EMBed 812 epoxy resin overnight under vacuum and the resin was polymerized at 60 °C for 48 h afterwards. The block of resin was trimmed first using a Leica EM Trim and then using a glass knife, resulting in a pyramid-like shape with a narrow window exposing the cross-section of the TFC samples. Ultrathin sections of 70 nm were obtained using a diamond knife on a Leica EM UC7 ultramicrotome device at room temperature. The angle of the knife was set at 6°, the step at 70 nm and the speed at 1 mm s^{-1}. The ultrathin sections were mounted on carbon 300 mesh copper grids, left to dry on a filter paper and then transferred to a grid box. Imaging of the TEM specimens was carried out using a Tecnai T20 TEM at an acceleration voltage of 200 kV.

A scanning electron microscope (SEM) FEI Quanta 250 FEG-SEM was used to study the cross-section and porosity of various polyacrylonitrile supports and TFC membranes of PIM-1 and cPIM-1. Samples for cross-sectional imaging were prepared by immersing the samples in DI water for 15 s, then introducing them into liquid nitrogen for another 15 s, where the membrane was fractured. The membranes were coated with 5 nm of Au/Pd (80:20) nanoparticles using a Pt/Au Quorum Sputter (UK), then left to dry for 3 h. The images were produced by utilizing a Secondary Electron (SE) detector. ImageJ software was used to perform size and area measurements on the PAN supports.

2.6. Gas permeance testing

2.6.1. Single gas permeance testing and ideal selectivity calculation

Single gas permeance testing was carried out using pure N_2, CH_4 and CO_2, in that sequence, by the standard variable volume method [32]. An upstream gauge pressure around 2.5 atm was maintained at room temperature, with the downstream permeate side at atmospheric pressure. Membranes were cut into circular coupons to fit the testing cell, with active permeation area of 2.84 cm^2. Before any test, membranes were pressure-conditioned for 20 min for self-standing membranes and for 5 min for TFC membranes (prepared on Sepro PA350 support) for each gas. At fixed pressure, the time for a specific volume of permeate gas was recorded for permeance calculation based on the following equation:

$$K = \frac{Q}{tA(p_1 - p_2)} \times 10^6 \tag{2}$$

where K is the gas permeance (GPU, 1 GPU = 10^{-6} cm^3 [STP] cm^{-2} s^{-1} $cmHg^{-1}$ = 3.348 × 10^{-10} mol m^{-2} s^{-1} Pa^{-1}), Q is the volume of penetrated gas (cm^3, corrected to STP [0 °C, 1 atm]), t is the permeation time (s), A is the active membrane permeation area (cm^2), and p_1 and p_2 are pressure in the membrane feed side and permeate side (cmHg), respectively. Membrane gas permeability was calculated by:

$$P = K \times l \tag{3}$$

P is the membrane permeability (barrer, 1 barrer = 10^{-10} cm^3 [STP] cm cm^{-2} s^{-1} $cmHg^{-1}$ = 3.348 × 10^{-16} mol m m^{-2} s^{-1} Pa^{-1}), l is the membrane thickness (μm). Membrane ideal gas selectivity was calculated as the ratio of gas permeance or gas permeability by:

$$\alpha_{CO_2/x} = \frac{K_{CO_2}}{K_x} = \frac{P_{CO_2}}{P_x} \tag{4}$$

where x is either N_2 or CH_4. TFC membranes were all tested as fresh samples unless mentioned otherwise. TFC membrane performances were tracked during a physical aging period of 60 days. Aged TFC membranes were further refreshed by storing them along with methanol-wetted tissue paper (kept in an open plastic bag to allow slow release of methanol vapor) in a sealed plastic zipper bag at room temperature for 7 days [53]. At least two membranes of each sample were tested for reproducibility, and the average with standard deviation is reported.

2.6.2. CO_2 pressure dependent measurement of TFC membranes

The effect of CO_2 pressure on separation performance was carried out with pure CO_2 using a similar dead-end gas permeation cell to that described above, but with an active permeation area of 8.7 cm^2. TFC membranes prepared on UF010104 PAN support (batch G) were tested from gauge pressure 1.4 bar–15 bar to track the CO_2 permeance change based on feed pressure.

2.6.3. Mixed gas testing

Mixed gas testing was carried out using a 10% CO_2/90% N_2 mixture under upstream gauge pressure around 2.5 and 4.8 bar at room temperature, with the downstream permeate side at atmospheric pressure. Cross gas flow (0.8–1 L/min) was maintained on the feed side to reduce

Table 1
D-PIM-1 and B-PIM-1 polymers produced from step growth polymerization in dilute solvent mixtures, from different temperature profiles; results from ^{1}H NMR and multi-detector GPC analysis.

Polymer sample[a]	Polymerization details[b]			^{1}H NMR analysis[c]	Multi detector GPC analysis[d]			
	Temp. Set/Av. (°C)	Time (min)	Yield (%)	Branching (%)	M_w (kg mol^{-1})	M_n (kg mol^{-1})	$Đ$	Intrinsic Viscosity (cm^3 g^{-1})
D-PIM-1	160/141	30	97.2	3.7	116	59.5	1.9	35.0
B-PIM-1	160/127	40	97.2	6.5	143	55.9	2.6	39.3

[a] D-PIM-1 denotes a predominantly di-substituted PIM-1 polymer, whereas B-PIM-1 refers to a more heavily branched PIM-1 polymer. Both polymers exhibit low network contents, below 2%.
[b] Set/average polymerization temperature, total reaction time and yield obtained in the respective polymerizations.
[c] Aromatic proton integral area analysis to provide estimation of the level of branching, based on the defect peaks attributed to branch points (**c** and **d**) compared as percentage of major peaks attributed to di-substituted PIM-1 residue structures (**a** and **b**) as outlined in Table S1.
[d] Molar mass distribution analysis of polymers in chloroform to obtain weight-average molar mass (M_w), number-average molar mass (M_n) and dispersity = M_w/M_n for the samples.

the concentration polarization effect [54]. The stage cut was less than 3%. The permeate gas composition was analyzed by gas chromatography using an Agilent 490 Micro GC (10 m PPU Heated Inj, column temperature 70 °C, injector temperature 40 °C). The mixed gas permeance was calculated using:

$$K_i = \frac{Qy_i}{tA(p_1x_i - p_2y_i)} \times 10^6 \quad (5)$$

where i represents either N_2 or CO_2, x is the mole fraction on the feed side and y is the mole fraction on the permeate side. K, Q, t, A, p_1 and p_2 are as defined above. Mixed gas selectivity was calculated as a ratio of permeances. Mixed gas separation factor (SF) was calculated using:

$$SF = \frac{y_{CO_2}x_{N_2}}{y_{N_2}x_{CO_2}} \quad (6)$$

where x_{CO_2} and x_{N_2} are the mole fractions of CO_2 and N_2 in the feed, respectively, and y_{CO_2} and y_{N_2} are the mole fractions of CO_2 and N_2 in the permeate, respectively. UF010104 PAN support (batch G) was used for the mixed gas study.

3. Results and discussion

3.1. PIM-1 synthesis and hydrolysis

Two PIM-1 samples, a predominantly di-substituted (D-PIM-1) and a more branched (B-PIM-1) polymer, with similar weight-average molar mass and negligible network content (below 2%) were produced in high yield polymerizations carried out at average temperatures of 141 and 127 °C, respectively (Table 1). Compared to previous work, 20 vol% more solvent was present at the beginning of each polymerization, altering the early temperature profile in these reactions, with two extra 20 vol% additions in the middle of the reactions ensuring uniform mixing throughout the remainder of the process and helping to avoid excessive network formation. However, excess solvent at the beginning, and later dilutions, made it more difficult to monitor the torque change on the overhead stirrer. The reaction quenching points were therefore more dependent on direct visual observation of mixing status. Once the solution became viscous and hard to mix, the reaction was stopped. Even though the hot plate temperature for both reactions was set at the same 160 °C, the short reaction time and different size of the heating block led to a 14 °C temperature difference on average, resulting in differences in topology as indicated in Fig. 1 and discussed below. Results of analysis by multi-detector GPC are included in Table 1. Both PIM-1 polymers showed high weight-average molar mass (M_w >100 kg mol^{-1}) with moderate dispersity ($Đ$ <3). Elemental analysis was conducted to confirm the –COOH conversion and is summarized in Table 2. Conversion to amide would result in very little change in terms of nitrogen content. All cPIM-1s synthesized in this work contained significantly decreased levels of nitrogen compared to PIM-1, which supported the presence of –COOH. The 48 h hydrolysis of B-PIM-1, which exhibited the lowest nitrogen content (0.52%) and equated to 90% conversion, was denoted as B-cPIM-1-90%. The 24 h hydrolysis reactions showed similar conversions of around 70–80%.

3.2. Polymer characterization

The ^{1}H NMR spectrum of D-PIM-1 (Fig. 3) is consistent with previous studies [55,56]. Resonances attributed to methyl protons show at 1.25 ppm and methylene protons at around 2.2 ppm. The aromatic protons are subdivided into two different peaks (**a** and **b**), due to the spiro-center of the TTSBI monomer, at 6.75 ppm and 6.35 ppm. When the polymerization is conducted at a lower temperature there are more mono-substituted connections giving rise to a branched structure, which is reflected in the ^{1}H NMR spectrum of B-PIM-1 (Fig. 3) with two minor peak shoulders (**c** and **d**) shown at 6.6 and 6.2 ppm, which are attributed to the aromatic protons adjacent to the branching –OH group [31,32].

Table 2
Elemental analysis of PIM-1s and cPIM-1s, and hydrolysis conversion calculations. Expected values for PIM-1 and fully hydrolyzed cPIM-1 are in bold.

Polymer	Hydrolysis time (h)	C (%)	H (%)	N (%)	N/C ratio	Conversion (%)[a]
PIM-1		**75.6**	**4.38**	**6.08**	**0.080**	**0**
D-PIM-1	0	73.4	4.23	6.15	0.084	0
B-PIM-1	0	73.5	4.20	6.09	0.083	0
D-cPIM-1-70%	24	66.5	4.51	1.63	0.025	70
B-cPIM-1-73%	24	67.1	4.63	1.46	0.022	73
B-cPIM-1-81%[b]	24	65.6	4.59	0.99	0.015	81
B-cPIM-1-90%	48	66.3	4.69	0.52	0.0078	90
cPIM-1		**69.9**	**4.45**	**0.00**	**0**	**100**

[a] Hydrolysis conversion was calculated based on N/C ratio change through the equation: $Conversion = \frac{(N/C\ ratio)_{PIM-1} - (N/C\ ratio)_{cPIM-1}}{(N/C\ ratio)_{PIM-1}} \times 100\%$.
[b] B-cPIM-1-81% was prepared in the same way as B-cPIM-1-73% but had slightly different conversion. Polymer characterization of B-cPIM-1-81% can be found in Supplementary Information Figs. S9, S11, S13 and S14.

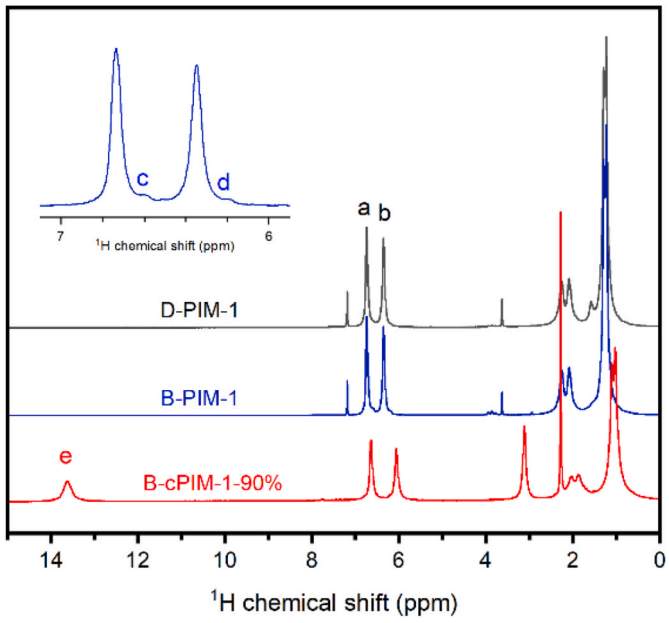

Fig. 3. ^{1}H NMR spectra of D-PIM-1 and B-PIM-1 in $CDCl_3$ and B-cPIM-1-90% in DMSO-d_6. The inserted figure is an amplified B-PIM-1 spectrum range from 6 to 7 ppm. The letters are related to the proton positions reflected in Figs. 1 and 2.

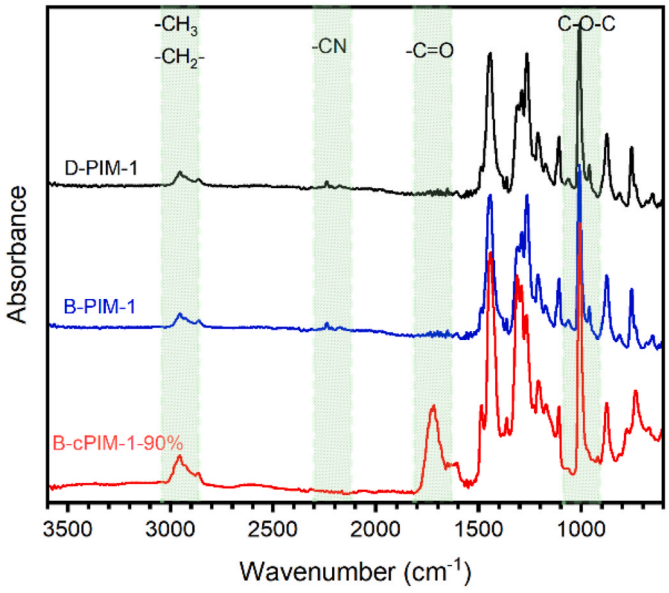

Fig. 4. FT-IR spectra of D-PIM-1, B-PIM-1, and B-cPIM-1-90% polymers.

The proportion of branching residues was calculated by comparing the integral areas of shoulder peaks (**c** and **d**) to the integral areas of main peaks (**a** and **b**), yielding a value of 6.5%. After 48 h acid hydrolysis of B-PIM-1, a peak appears at 13.6 ppm in the ^{1}H NMR spectrum (Fig. 3), which is representative of a carboxylic acid proton (**e**) in B-cPIM-1-90%, rather than an amide proton, which typically arises at 7–8 ppm [39]. Full ^{1}H NMR spectra of polymers synthesized in this work are presented in Fig. S2, S3, and S7–S10.

FT-IR spectra are presented in Fig. 4 and Fig. S11. There was little difference between the FT-IR spectra of B-PIM-1 and D-PIM-1 polymer samples, similar to previous reports [45,57]. Peaks at around 1007 and 2950 cm^{-1} are related to the stretching of the dioxane group (C–*O*–C) and alkyl groups (-CH_3, –CH_2-) of PIM-1, respectively. The small sharp peak at 2234 cm^{-1} is a typical nitrile (-CN) stretching. The branching

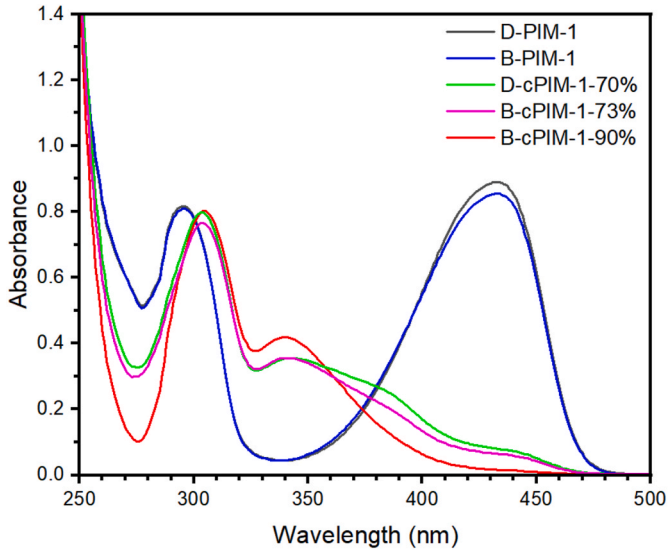

Fig. 5. UV–Vis absorption spectra of PIM-1s and cPIM-1s, obtained from 0.09 mM THF solutions.

hydroxy group is not obvious in the spectra, probably due to the low content. The nitrile group decreases or disappears after hydrolysis, with a new carboxylic acid – carbonyl (–C═O) stretch arising at 1710 cm^{-1}, rather than forming an amide carbonyl stretch at 1650 cm^{-1} [42].

Polymers were also characterized in solution in THF by UV–Vis spectroscopy (Fig. 5). The absorption at 433 nm is partially related to the π-π* conjugation [31] of five fully fused aromatic rings (6,13-dicyano-benzo-1,2,4',5'-bis-1,4-benzodioxane chromophores) between the spiro-centres in the di-substituted PIM-1 structure. However, each branch point disrupts this conjugated structure, leading to a decreased absorption at 433 nm. The lower absorbance obtained for B-PIM-1, compared to D-PIM-1 at 433 nm, shown in Fig. 5, supports the branched structure formation in that sample. The conversion from –CN group to –COOH group also leads to a color change from bright yellow to brown. The main –CN absorption at 433 nm diminishes after hydrolysis and the absorption of –COOH at 378 nm rises [42]. Longer hydrolysis time (24 h vs. 48 h) is associated with higher conversion, accompanied with lower –CN and higher –COOH absorption. The relative difference at 433 nm between D-cPIM-1-70% and B-cPIM-1-73% again supports the disruption of π-π* conjugation by the branch points.

In DLS analysis (Figs. S12 and S13) all polymers exhibit similar size

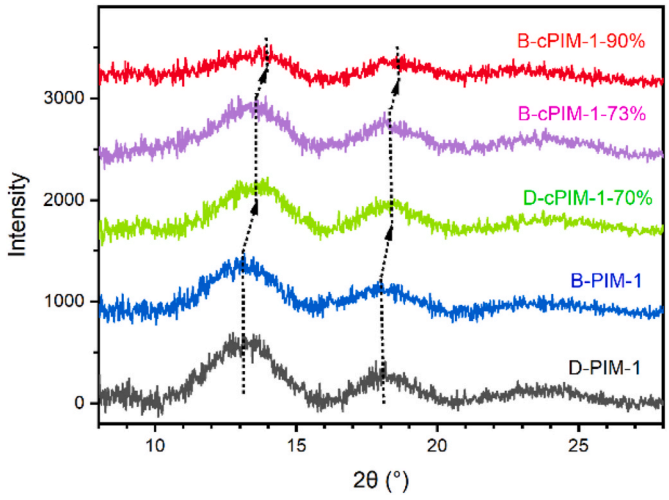

Fig. 6. XRD analysis of powder samples of PIM-1s and cPIM-1s.

(hydrodynamic diameter) distribution in terms of both intensity and number. All number-average particle sizes of the diluted dispersion in THF are around 10–15 nm. The size distributions indicate no large aggregates that typically appear at a size of more than 100 nm with significant number percent.

Polymer powder samples were characterized by XRD as shown in Fig. 6. Two obvious peaks around 13° (*d*-spacing = 6.8 Å) and 18° (*d*-spacing = 4.9 Å) may be attributed to the distances between loosely packed chains and micropores of the ladder-structured polymer, respectively [44,46,58]. The structural difference evident in the two PIM-1 samples was not reflected in the respective diffraction peaks. However, the *d*-spacing decreased as the hydrolysis proceeded from 0 to 48 h, which may be attributed to more intense polymer chain interactions produced by the –COOH rich environment. This change would favor CO_2 permeation over N_2 and CH_4 as will be demonstrated in the following section.

TGA was performed on all polymers as shown in Fig. 7 and Fig. S14. Each sample had an isothermal pre-treatment at 150 °C for 1 h to remove any residual water and solvent. Both the di-substituted and the branched PIM-1 polymers were thermostable and significant weight loss only started to occur around 500 °C, related to the polymer backbone decomposition [59,60]. The slightly greater weight loss for B-PIM-1 compared to D-PIM-1 indicated that the structure richer in mono-substituted linkages is less stable than a predominantly di-substituted polymeric structure. For all carboxylated PIM-1s, two stages of weight loss are observed. The weight loss of the first stage around 300 °C–450 °C is due to the decomposition of –COOH groups. For a fully carboxylated PIM-1, this weight loss should equate to 18%. Based on this assumption, 12% weight loss of D-cPIM-1-70% and B-cPIM-1-73% and 14% weight loss of B-cPIM-1-90% indicate approximate hydrolysis conversions of 67% and 78%, respectively, representing a small discrepancy from the elemental analysis determination. The –COOH loss of B-cPIM-1-90% starts at a higher temperature than the 24 h hydrolyzed PIM-1, which suggests the greater content of –COOH produces a more stable structure by the rich H-bonding environment. The interaction can intensify the chain packing of polymer under TFC membrane conditions, which will be demonstrated later.

3.3. Single gas permeability of self-standing membranes

PIM-1s and cPIM-1s were firstly prepared as self-standing membranes for permeability testing. However, all cPIM-1s proved brittle and particularly hard to retest to obtain aging data, which might be due to the intense H-bonding effect. In particular, the product of the 48 h hydrolysis of the branched PIM-1 sample, B-cPIM-1-90%, could not be initially cut into a coupon to fit the testing rig. By contrast, it has been reported that the long-term base hydrolyzed PIM-1, which also proved to have high COOH conversion [39], can be cast into self-standing membranes which still maintain a yellowish color and are flexible. The thick film CO_2, N_2 and CH_4 permeation data for PIM-1s and cPIM-1s are compiled in Table S2 and data from individual membranes can be viewed in Table S3. The CO_2/N_2 performances are shown in a Robeson plot in Fig. 8. The initial gas permeability and selectivity for both types of PIM-1 (1 day aging) proved identical within experimental error, with CO_2 permeability recorded at nearly 9000 barrer and CO_2/N_2 selectivity around 12. B-PIM-1 membranes maintained 30% of their initial CO_2 permeability after 145 days aging and had a slightly better aging performance than their D-PIM-1 counterparts, which only maintained 23% of their initial CO_2 permeability. The aging behavior followed the Robeson upper bound slope (grey arrow in Fig. 8). All cPIM-1 membranes showed significantly improved CO_2/N_2 ideal selectivity, more than 40, but reduced gas permeability, around 400 barrer of CO_2. This is attributed to a more intense H-bonding network and overall densified polymer structure producing a better molecular sieving ability that favors CO_2 permeation [40].

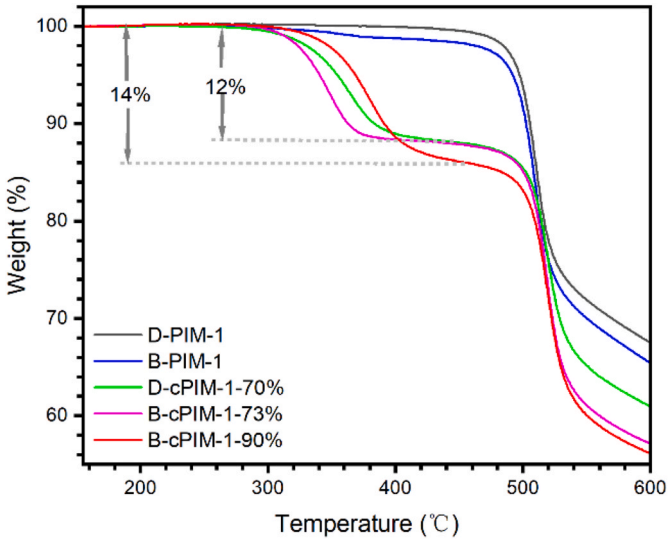

Fig. 7. TGA traces obtained from powder samples of PIM-1s and cPIM-1s. Weight losses of D-cPIM-1-70%, B-cPIM-1-73% and B-cPIM-1-90% at first stage are labeled.

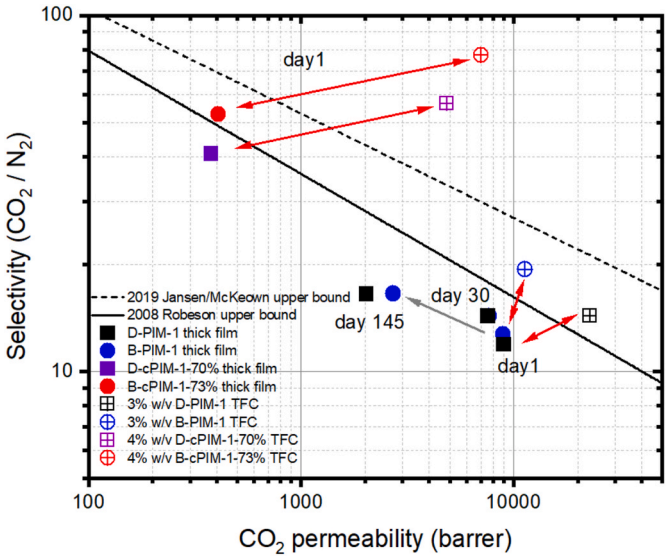

Fig. 8. Robeson plot with Robeson 2008 upper bound (solid line) [14] and Jansen/McKeown 2019 upper bound (dashed line) [15], showing CO_2 and N_2 single gas derived membrane performance of thick films of D-PIM-1 and B-PIM-1 aged for 1, 30 and 145 days, and of hydrolyzed samples, D-cPIM-1-70% and B-cPIM-1-73% after 1 day aging. For comparison, initial TFC performance of all these materials after 1 day is also included. The grey arrow indicates the thick PIM-1 film aging trend and the two-way red arrows indicate performance comparisons between thick film and thin film composite membranes prepared from the same material. (For interpretation of the references to color in this figure legend, the reader is referred to the Web version of this article.)

3.4. Single gas permeance of thin film composite membranes

TFC membranes for initial single gas studies were prepared by a kiss-coating method on Sepro PA350 support. In general, the solvents used for coating do not significantly affect the permeance of a PAN support (see Table S4), although some supports are more sensitive than others to the coating process, as mentioned later. PIM-1 TFC membranes were prepared from 3% w/v coating solution in THF. The viscosity of cPIM-1 coating solution decreased with increasing hydrolysis conversion. This meant that a 3% cPIM-1 coating solution failed to form a complete

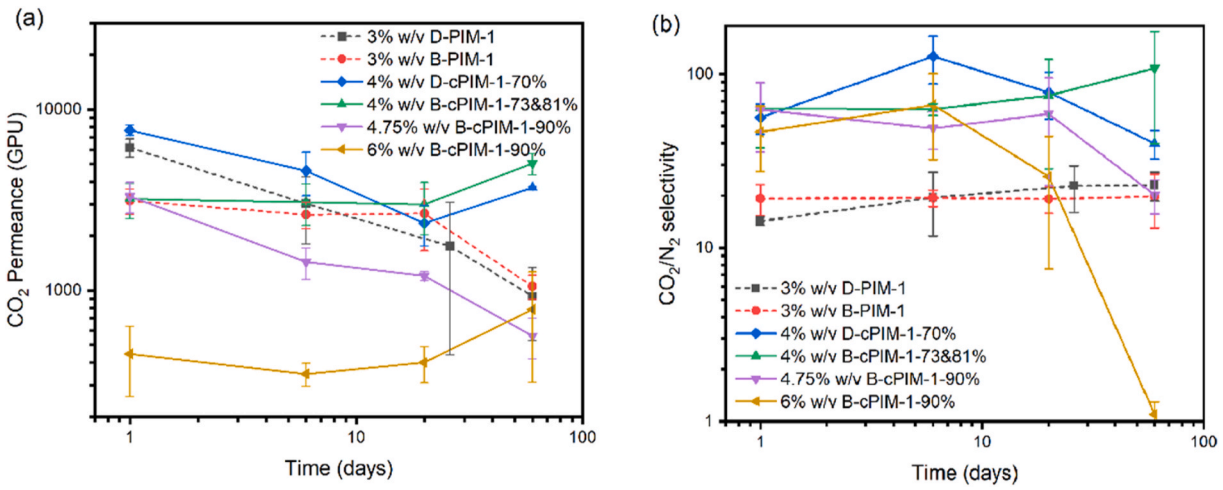

Fig. 9. (a) CO_2 permeance and (b) CO_2/N_2 ideal selectivity aging data of TFC membranes formed from D/B-PIM-1 with 3% (w/v) coating concentration, D-cPIM-1-70%, B-cPIM-1-73&81% with 4% (w/v) coating concentration, and B-cPIM-1-90% with 4.75% (w/v) and 6% (w/v) coating concentration, respectively.

selective layer on top of the PAN support, so higher concentrations were used, namely 4% for D-cPIM-1-70%, B-cPIM-1-73% and B-cPIM-1-81% (B-cPIM-1-73% and B-cPIM-1-81% were both prepared by 24 h acid hydrolysis; where data are combined as an average when specified as B-cPIM-1-73&81%) and two higher coating concentrations, 4.75% and 6%, for B-cPIM-1-90%. The aging behavior of averaged data is summarized in Fig. 9, Fig. S15 and Table S6, and separation performance of individual coupons can be viewed in Tables S7–S12. The thin active layer in a TFC membrane usually experiences rapid physical aging effects that manifest in a few weeks, but which can take months or even years in thick film membranes [19]. Structural rearrangement occurs more easily with a thinner active layer, allowing faster approach towards a thermodynamic equilibrium state [21], with its decreased free volume and lower gas permeability. The di-substituted structure, either D-PIM-1 or D-cPIM-1-70%, exhibits normal TFC membrane aging behavior, with a dramatic permeance decrease within the first six days and slower permeance decrease thereafter. The CO_2 permeance of D-PIM-1 and D-cPIM-1-70% falls by 85% and 52%, respectively, after 60 days. However, the branched structure has better anti-aging properties. The B-PIM-1 polymer, proposed to exist as a multi-branched polymeric structure, containing very little colloidal network content [33], showed only 15% and 65% CO_2 permeance decreases after 20 and 60 days, respectively. Appropriate degree of carboxylation of this polymer proved to maintain the original branched structure performance. B-cPIM-1-73&81% showed quite stable performance over 60 days in terms of both gas permeance and selectivity. However, by comparison, highly hydrolyzed B-cPIM-1-90% TFC samples coated from 4.75% sample solution tended to have rapid permeance fall at an early stage, which suggests that rapid structure densification by strong H-bonding interactions occurs in an extremely –COOH rich environment (see discussion of TGA). B-cPIM-1-90% TFC membranes coated from a higher concentration solution of 6% yielded a comparatively thicker selective layer (both shown in the TEM analysis presented in Fig. 10) exhibiting CO_2 permeance of about 400 GPU. The steady CO_2 permeance over 20 days was accompanied by decreased selectivity, and even a loss in all selectivity at the end, which could be ascribed to the membrane

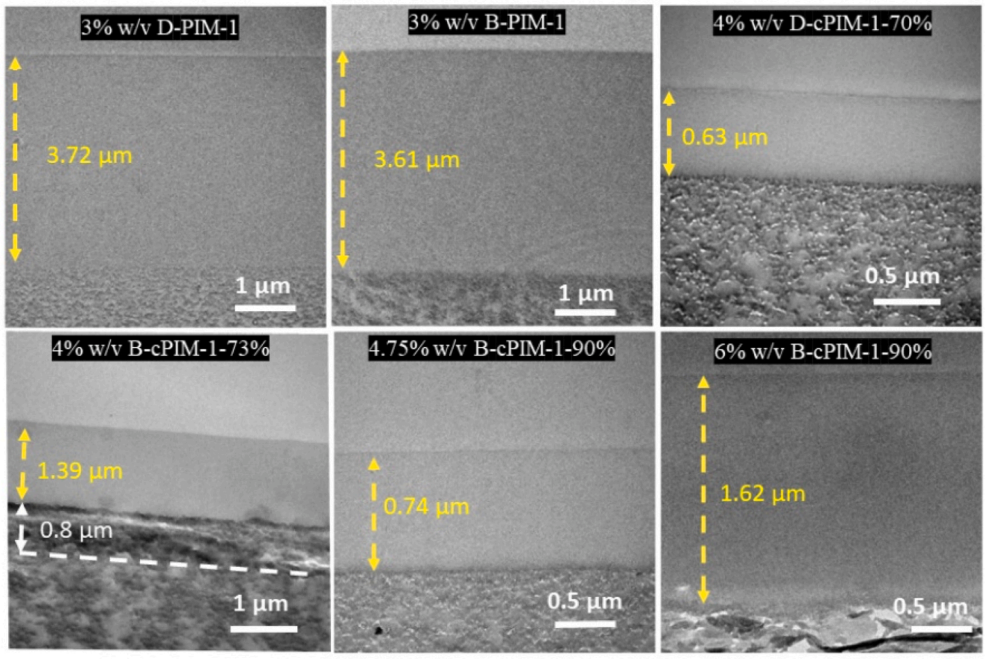

Fig. 10. Cross-sectional TEM images of TFC membranes prepared from 3% w/v solutions of D-PIM-1 and B-PIM-1, along with TFC membranes prepared from 4% w/v solutions of D-cPIM-1-70% and B-cPIM-1-73%, and TFC membranes of B-cPIM-1-90% prepared from both 4.75% w/v and 6% w/v coating solution. White dashed line indicates level of solution penetration and yellow dashed line indicates surface layer thickness. (For interpretation of the references to color in this figure legend, the reader is referred to the Web version of this article.)

breaking and leaking, probably due to increased material brittleness brought on by membrane aging. Changes in CO_2 permeability over time for B-PIM-1 and B-cPIM-1-73&81% TFC membranes are compared with other topologically different PIM-1 TFC membranes in Fig. S16, and initial aging rates ($-\partial \log P/\partial \log t$) [61,62] are given in Table S5. B-PIM-1 and B-cPIM-1-73%&81% TFC membranes exhibit minimal initial aging compared to PIM-1 TFC membranes studied previously [31,34,63].

Both PIM-1s produced TFC membranes with a similar CO_2/N_2 selectivity around 20. cPIM-1 TFC membranes exhibited significantly improved ideal selectivity, above 45. The selective performance of B-cPIM-1-73&81% was more stable over the aging test, however the more fully hydrolyzed B-cPIM-1-90% underwent similar aging behavior to D-cPIM-1-70%, showing decreased selectivity at the end.

TFC membranes of polymers that were both hydrolyzed and branched were prepared from two different batches, B-cPIM-1-73% and B-cPIM-1-81%, and in total 15 fresh membrane coupons were tested over 60 days' aging. The lowest ideal CO_2/N_2 selectivity of all coupons tested was still greater than 40 and some selectivities exceeded 100, which accounts for the large selectivity error bars. Given that the cPIM-1 polymers were coated from THF, which is hygroscopic, and that the polymer itself may adsorb some moisture, it is possible that traces of water in the membranes contribute to variations in selectivity. The full data can be examined in Table S10.

Cross-sectional TEM images of a selection of the TFC membranes, with the calculated surface active layer thickness values (marked in yellow), are shown in Fig. 10. Both D-PIM-1 and B-PIM-1 show similar thickness of 3.72 μm and 3.61 μm, respectively. These surface active layers are thicker than reported in a previous publication [31,34], which indicated an average of 2 μm for all PIM-1 TFC membranes with almost the same coating procedure, except that a larger roller coater and THF solvent were used in this work. The lower initial permeance observed for B-PIM-1 TFC, when multiplied by its surface active layer thickness, equated to membrane permeability in the range of 11–12,000 barrer, as typically previously reported for PIM-1 TFC membranes [31,34]. Thick films cast from the two PIM-1 samples in chloroform exhibited slightly lower initial permeabilities of around 9000 barrer. The solution viscosity of the di-substituted sample is higher than the branched sample in the hydrolyzed state, which impacts interactions with the PAN support. Starting from 4% w/v coating concentrations, 0.63 μm and 1.39 μm surface active layer thicknesses, on top of the PA350 support, were obtained from D-cPIM-1-70% and B-cPIM-1-73%, respectively. The TEM analysis of the 4% w/v B-cPIM-1-73% TFC also showed some evidence of partial penetration (marked in white, approx. 0.8 μm) into the underlying PAN support. All thin film permeabilities (calculated by multiplication of the respective permeance and effective active layer thickness in microns in each case) significantly improved compared with the thick film (Fig. 10, Table S13), especially for cPIM-1s less than 90% hydrolyzed, which had material permeabilities more than tenfold greater than those found in thick films. As with PIM-1, some of this increased initial permeability found for cPIM-1 TFC membranes, compared to comparable thick films, can be attributed to the mode of film formation. In thick film formation, the solvent is allowed to evaporate slowly. However, in thin film formation, the solvent can evaporate very rapidly [64] and potentially leaves an initially more loosely packed structure. This loosely packed structure in TFC membranes would possess more free volume and produce a higher CO_2 permeability. The most significant contribution to the inflated single gas CO_2 permeabilities may prove to be attributable to increased plasticization occurring in the partially hydrolyzed cPIM-1 TFC membranes, which will be discussed in more detail later. By contrast, the more fully hydrolyzed cPIM-1-90% TFC membranes coated from 6% w/v solutions actually exhibited initial permeability much more closely aligned to their equivalent thick film.

TFC membranes of cPIM-1 often exhibited large variations in high ideal selectivity between individual coupons, which contribute to sometimes large standard deviations. Two particular membrane coupons prepared from 4% w/v B-cPIM-1-81% solution, measured after 60 days aging, with similar CO_2 permeance (coupon A 4600 GPU vs. coupon B 5500 GPU) but significantly different CO_2/N_2 selectivity (coupon A 60 vs. coupon B 160), were selected to be characterized by TEM (Fig. S17). TEM analysis had previously shown significant penetration of polymer into the support for 4% w/v B-cPIM-1-73% solution (Fig. 10). In comparing these two additional coupons, it is possible to discern that in the case of coupon B the coating solution has again partially penetrated into the support (marked in white, approx. 0.7 μm), causing additional transport resistance [65]. The overall similar cPIM-1 layer thickness (layer on support surface plus penetration layer) resulted in a similar CO_2 permeance. However, the N_2 permeability is significantly reduced where there is penetration into the pores of the support, leading to higher CO_2/N_2 selectivity. This has been observed previously by Chernova et al. [66] in studies of PIM-1 constrained in the pores of anodic alumina membranes. Confinement of the polymer chains within a small pore reduces polymer mobility, hindering diffusion of permanent gases for which transport is diffusion-controlled, but with less effect on condensable gases for which transport is solubility-controlled.

The TFC membrane CO_2/N_2 performances are collated for comparison to the industrially favored region in Fig. 11. Comparisons with other state-of-the-art work published in the literature are presented in Fig. S18 and Table S14. Compared to self-standing membranes, typically with thicknesses of more than 50 μm, TFC membranes are more attractive because the overall asymmetric structure allows a thin active layer, thus significantly reducing the mass transfer resistance and increasing the gas throughput. Recently, research has focused on building thinner and thinner active layers by using either surface polymerization [23,25] or developing suitable materials [28], and the resulting thin layer has reached a level below 100 nm. In this work, ultra-permeable cPIM-1 TFC membranes are fabricated, simply using solution processable polymer and a kiss coating method, directly on a PAN support without introducing a gutter layer, which is applicable to an industrial scale. Even though active layer thicknesses are on the micrometer scale, the ideal gas separation performance still falls comfortably within the target range. By introducing a branched structure and the necessary amount of hydrolysis to that PIM-1 polymer, the severe aging problems often associated with PIM-1 membrane materials can be mitigated. However, ideal selectivities from single gas measurements may differ markedly

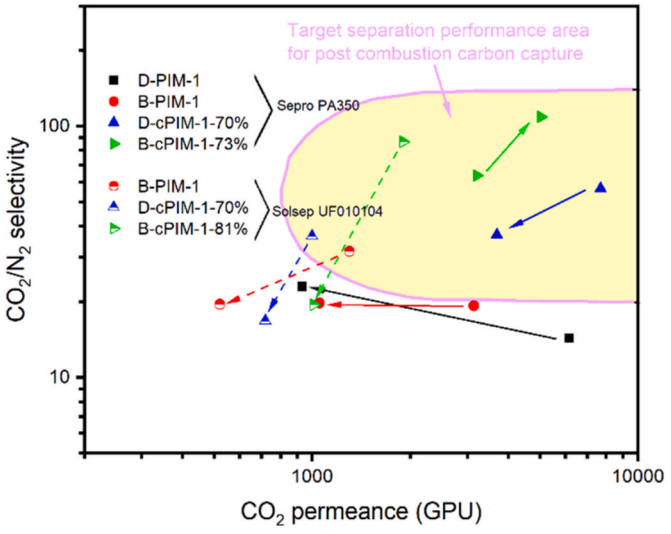

Fig. 11. Comparison of the CO_2/N_2 separation performances of TFC membranes of PIM-s and cPIM-1s prepared in this work with the industrial favored range suggested by Merkel et al. [18] for post-combustion carbon capture. The solid symbol and solid arrows indicate the trends of 60 days aging of TFC membranes prepared from Sepro PA350 support, and the half-filled symbols and dash arrows indicate the performance shift from single gas to mixed gas of TFC membranes prepared from Solsep UF010104 support.

from those realizable in practice with gas mixtures, because strongly sorbing gases such as CO_2 may plasticize the polymer. This is discussed further below.

3.5. Pressure dependence and mixed gas performance of thin film composite membranes

Glassy polymers are prone to plasticization, where a highly-sorbing penetrant such as CO_2 modifies the interactions between polymer chains and enhances the chain mobility, leading to an increase in free volume. In a gas separation membrane, this is generally manifested as an increase in permeability with increasing pressure, sometimes above a minimum pressure referred to as the plasticization pressure. For gas mixtures, plasticization usually leads to a decrease in selectivity. Plasticization effects, which may arise even with "rigid" PIMs [67], can be particularly pronounced in thin films [64,68,69].

In the present work, plasticization effects were investigated for TFC membranes of PIM-1 and hydrolyzed PIM-1 on a SolSep UF010104 PAN support (batch G). It should be noted that there are differences between this support and the Sepro PA350 support used in the work described above, the SolSep support being more prone to loss in porosity during the coating procedure (see SEM analysis presented in **SI**, Figs. S19–S21, Tables S15–S16). Fig. 12 shows that there is an increase in CO_2 permeance with increasing pressure for both B-PIM-1 and B-cPIM-1-81% TFC membranes, indicating significant plasticization in thin films (data collated in Table S17). The CO_2 permeance approximately doubled as feed pressure increased from 1.4 bar to 15 bar. Similar plasticization behavior has been reported by Tiwari et al. [70] for a 1 μm self-standing PIM-1 thin film. In contrast, for PIM-1 thick films (50–100 μm), Li et al. [71] and Swaidan et al. [67] observed a decrease in CO_2 permeability with increase in pressure up to 10 bar, reflecting a decrease in solubility coefficient with increasing pressure as expected for the dual-mode sorption model.

Table 3 gives gas permeation results for a mixture of 10% CO_2 in N_2 for TFC membranes of B-PIM-1, B-cPIM-1-81% and D-cPIM-1-70%, along with ideal gas selectivities from single gas measurements at 2.5 bar. It is clear that mixed gas selectivities are significantly lower than ideal selectivities, and that under these conditions the performance of the hydrolyzed PIM-1 is similar to that of the parent polymer. Some loss of selectivity may be a consequence of concentration polarization, where selective transport leads to a concentration gradient near the membrane surface, but this was minimized by maintaining a high cross gas flow on the feed side and keeping the stage cut below 3%. It is noteworthy that although the CO_2/N_2 mixed gas selectivity decreases with increasing pressure, at this modest concentration of CO_2 in the feed the separation factor nevertheless increases with increasing pressure. The cPIM-1 TFC membranes can concentrate CO_2 from 10% CO_2/90% N_2 feed to 28% and 38% at feed pressures of 2.5 bar and 4.8 bar, respectively.

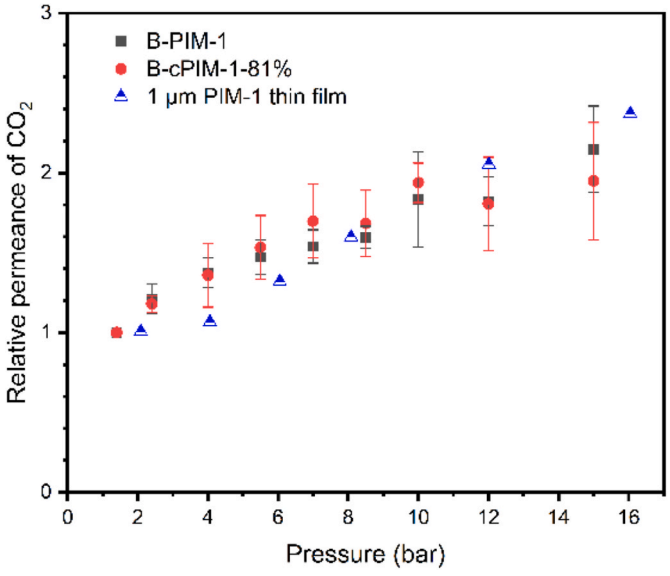

Fig. 12. Pressure dependence of CO_2 permeance (relative to value obtained at the lowest pressure) for B-PIM-1 and B-cPIM-1-81% TFC membranes from single gas testing (raw data can be viewed in Table S17). Data from Tiwari et al. [70] for a 1 μm PIM-1 self-standing thin film are included for comparison.

Strong plasticization has previously been observed in propene/propane separation with various polymers [64,72]. Lee et al. [64] investigated a range of glassy polymers and demonstrated more intense plasticization on decreasing the active layer thickness in TFC membranes, leading to poor mixed gas selectivities in thin films compared to isotropic bulk films. They utilized an additional plasticization-resistant coating to minimize plasticization and improve mixed gas selectivities. Ren et al. [72] studied amidoxime-functionalized PIM-1 as bulk films and reported that coordination crosslinking with metal ions could improve the plasticization resistance, however, the applicability of that approach to thin films has not yet been established.

The present work confirms that for CO_2 separations the mixed gas performance in thin films may deviate significantly from the ideal behavior of the bulk polymer. This highlights the importance of studying materials for gas separation membranes under mixed gas conditions in commercially-relevant thin films. Future work will investigate strategies for minimizing plasticization under these conditions.

3.6. Thin film composite membrane refreshment through methanol vapor treatment

B-cPIM-1-73&81% TFC membranes showed good aging performance during 60 days of physical aging, while the other TFC membranes still underwent significant physical aging when stored under ambient conditions in a sealed plastic zipper bag. It was found that when an aged TFC membrane that had been tested previously was retested, it gave a lower permeance than a similarly aged membrane that had not been tested previously. Liquid alcohol treatment is commonly used to recover free volume lost during aging of self-standing membranes [73,74]. However, this method cannot be utilized to refresh a TFC membrane due to the risk of membrane delamination. An alcohol vapor treatment has also been used to regenerate self-standing membranes [75] and TFC membranes [21]. In this work, a facile methanol vapor treatment method [53] was used to refresh TFC membranes aged more than six months (Table 4). Methanol vapor was allowed to diffuse into the membrane, which is expected to swell the PIM-1, leaving it in a higher free volume state. The permeance was at least partially recovered for all TFC membranes, although this was not as effective for the predominantly disubstituted structure as for the more branched structure, which may be attributed to reinforced intermolecular interactions in a disubstituted structure after fast initial densification. The performance of cPIM-1 TFC membranes on Sepro PA350 support that were aged for 200 days then refreshed was better than when previously retested after 60 days. For example, refreshed D-cPIM-1-70% gave a CO_2 permeance of 3400 GPU, 70% higher than the day 60 value, with CO_2/N_2 selectivity of 54, comparable to the day 1 value.

4. Conclusions

A series of thin film composite membranes have been prepared using PIM-1 and cPIM-1 polymers by a simple kiss coating method on PAN supports. PIM-1 TFC membranes with active layer thickness around 3.6 μm were obtained with CO_2 permeance in the range 3000–6000 GPU and CO_2/N_2 ideal selectivity around 20. cPIM-1 with hydrolysis degree of 70–80%, even though 20 times less permeable than PIM-1 when cast into thick films, can be successfully fabricated into 1 μm TFC membranes with similar CO_2 permeance to traditional PIM-1 TFC membranes (in the

Table 3
Mixed gas separation performance of TFC membranes of B-PIM-1, B-cPIM-1-81% and D-cPIM-1-70% from 10% CO_2/90% N_2 feed, and comparison with single gas performance.

Sample	Gauge pressure (bar)	Mixed gas permeance (GPU)		CO_2/N_2 mixed gas selectivity	Separation factor	Single Gas Permeance (GPU)	CO_2/N_2 ideal gas selectivity[a]
		N_2	CO_2			CO_2	
B-PIM-1	2.5	27 ± 14	520 ± 177	19.6 ± 3.4	3.5 ± 0.1	1300 ± 350	31.8 ± 6.7
	4.8	31 ± 11	516 ± 251	16.3 ± 2.7	5.6 ± 0.2		
B-cPIM-1-81%	2.5	52 ± 8	1012 ± 182	19.5 ± 3.1	3.6 ± 0.1	1900 ± 410	86.7 ± 8
	4.8	68 ± 9	881 ± 63	13.2 ± 1.4	5.3 ± 0.1		
D-cPIM-1-70%	2.5	44 ± 11	717 ± 32	16.8 ± 4.8	3.5 ± 0.2	1000 ± 320	36.5 ± 6.4
	4.8	52 ± 15	708 ± 174	13.6 ± 0.7	5.4 ± 0.2		

[a] Idea gas selectivity was obtained at 2.5 bar through single gas testing. Detailed data can be viewed in Table S17.

Table 4
Thin film composite membrane performance of D-PIM-1, B-PIM-1, D-cPIM-1-70% and B-cPIM-1-73% at day 1, day 60 and after methanol vapor refreshment.

Sample	Aging (days)	Single gas permeance (GPU)			Ideal gas selectivity	
		N_2	CH_4	CO_2	CO_2/N_2	CO_2/CH_4
3% w/v D-PIM-1	1	430 ± 46	830 ± 100	6200 ± 720	14 ± 0.8	7.5 ± 0.6
	60	39 ± 13	52 ± 25	930 ± 400	23 ± 4.3	19 ± 1.9
	175 (refreshed)[b]	120 ± 23	220 ± 40	1800 ± 2100	16 ± 1.3	8.5 ± 0.6
3% w/v B-PIM-1	1	170 ± 61	300 ± 120	3100 ± 490	19 ± 3.9	11 ± 2.9
	60	58 ± 23	91 ± 20	1100 ± 160	20 ± 6.8	12 ± 1
	195 (refreshed)[b]	180 ± 50	340 ± 110	2300 ± 600	13 ± 1.9	6.9 ± 1
4% w/v D-cPIM-1-70%	1	140 ± 44	210 ± 68	7700 ± 507	57 ± 15	36 ± 11
	60 (retest)[a]	84 ± 84	110 ± 121	2000 ± 1300	29 ± 19	24 ± 13
	200 (refreshed)[b]	64 ± 7	90 ± 22	3400 ± 120	54 ± 3.5	40 ± 8.3
4% w/v B-cPIM-1-73%	1	40 ± 11	53 ± 9	2900 ± 130	77 ± 25	55 ± 10
	60 (retest)[a]	23 ± 7	31 ± 12	1000 ± 290	49 ± 24	39 ± 20
	200 (refreshed)[b]	40 ± 11	57 ± 22	1900 ± 41	50 ± 13	37 ± 14

[a] Performance of 4% w/v D-cPIM-1-70% and B-cPIM-1-73% at day 60 was obtained by characterizing samples already tested before.
[b] Performance of refreshed membranes was obtained by characterizing tested samples refreshed through methanol vapor treatment.

range 3000–7000 GPU), but significantly increased CO_2/N_2 ideal selectivities of around 60–100.

Both hydrolysis and introduction of a branched structure were able to mitigate membrane aging. In particular, B-cPIM-1-73&81% TFC membranes maintained a stable performance during 60 days' aging. Some of the significant enhancement in cPIM-1 separation properties of TFC membranes, compared to that of thick films, might be ascribed to fast solvent evaporation during film formation. This could leave a relatively loosely packed structure that ages differently to the structure formed by the slow solvent evaporation process (2–3 days) used to form self-standing films.

B-cPIM-1-73&81% TFC membranes exceeded the ideal performance of any other previously reported PIM-1 based TFC membranes, but still suffered from strong plasticization, which leads to a decreased gas separation performance under mixed gas conditions compared with single gas tests, similar to B-PIM-1. The effects of long-term physical aging of TFC membranes could partially be reversed through a methanol vapor treatment. The interaction between the support and coating polymer solutions, alongside the solvent evaporation behavior, and methods to mitigate plasticization effects, are deserving of further investigation in the quest to develop high performance TFC membranes.

CRediT authorship contribution statement

Ming Yu: Conceptualization, Investigation, Methodology, Data Curation, Writing – Original Draft. Andrew B. Foster: Conceptualization, Investigation, Methodology, Writing – Review & Editing. Mustafa Alshurafa: Investigation (scanning electron microscopy), Methodology, Writing – Review & Editing. Jose Luque-Alled: Investigation (transmission electron microscopy), Methodology, Writing – Review & Editing. Patricia Gorgojo: Supervision, Methodology, Writing – Review & Editing. Sandra E. Kentish: Supervision, Methodology, Writing – Review & Editing. Colin A. Scholes: Conceptualization, Funding acquisition, Supervision, Methodology, Writing – Review & Editing. Peter M. Budd: Conceptualization, Funding acquisition, Supervision, Methodology, Writing – Review & Editing.

Declaration of competing interest

The authors declare that they have no known competing financial interests or personal relationships that could have appeared to influence the work reported in this paper.

Data availability

Data supporting this study are available within the article and supporting materials.

Acknowledgments

Ming Yu is grateful to the University of Melbourne for a Melbourne Research scholarship for a dual award PhD programme between the University of Melbourne and the University of Manchester. Andrew B. Foster and Peter M. Budd acknowledge the support of EPSRC Programme Grant ep/v047078/1 "SynHiSel". Mustafa Alshurafa acknowledges the Department of Research & Development, Saudi Aramco, for PhD sponsorship. Patricia Gorgojo is supported by Grant RYC2019-027060-I funded by MICIN/AEI/10.13039/501100011033 and by "ESF Investing in your future". Jose Miguel Luque-Alled acknowledges the Spanish Ministerio de Economía y Competitividad and the European Social Fund for his Margarita Salas Fellowship. Authors acknowledge the use of instrumentation as well as the technical advice provided by the National Facility ELECMI ICTS, Laboratorio de Microscopias Avanzadas (LMA) at Universidad de Zaragoza.

Appendix A. Supplementary data

Supplementary data to this article can be found online at https://doi.org/10.1016/j.memsci.2023.121697.

References

[1] H.D. Matthews, N.P. Gillett, P.A. Stott, K. Zickfeld, The proportionality of global warming to cumulative carbon emissions, Nature 459 (2009) 829–832.
[2] K.O. Yoro, M.O. Daramola, CO_2 emission sources, greenhouse gases, and the global warming effect, in: Advances in Carbon Capture, 2020, pp. 3–28.
[3] F. Cherubini, G.P. Peters, T. Berntsen, A.H. Stromman, E. Hertwich, CO_2 emissions from biomass combustion for bioenergy: atmospheric decay and contribution to global warming, Gcb Bioenergy 3 (2011) 413–426.
[4] C.Z. Liang, T.S. Chung, J.Y. Lai, A review of polymeric composite membranes for gas separation and energy production, Prog. Polym. Sci. 97 (2019), 101141.
[5] Y. Han, W.S.W. Ho, Polymeric membranes for CO_2 separation and capture, J. Membr. Sci. 628 (2021), 119244.
[6] P.M. Budd, B.S. Ghanem, S. Makhseed, N.B. McKeown, K.J. Msayib, C. E. Tattershall, Polymers of intrinsic microporosity (PIMs): robust, solution-processable, organic nanoporous materials, Chem. Commun. (2004) 230–231.
[7] M.A. El-Okazy, L. Liu, C.P. Junk, E. Kathmann, W. White, S.E. Kentish, Gas separation performance of copolymers of perfluoro(butenyl vinyl ether) and perfluoro(2,2-dimethyl-1,3-dioxole), J. Membr. Sci. 634 (2021), 119401.
[8] I. Hossain, S. Park, A. Husna, Y. Kim, H. Kim, T.H. Kim, PIM-PI-1 and poly(ethylene glycol)/Poly(propylene glycol)-based mechanically robust copolyimide membranes with high CO_2-selectivity and an anti-aging property: a joint experimental-computational exploration, ACS Appl. Mater. Interfaces 13 (2021) 49890–49906.
[9] Y.T. Weng, Q.X. Li, J.X. Li, Z. Gao, L. Zou, X.H. Ma, Facile synthesis of Bi-functionalized intrinsic microporous polymer with fully carbon backbone for gas separation application, Sep. Purif. Technol. 279 (2021), 119681.
[10] Z.L. Cai, Y.T. Liu, C. Wang, W. Xie, Y. Jiao, L.L. Shan, P.Y. Gao, H.T. Wang, S. J. Luo, Ladder polymers of intrinsic microporosity from superacid-catalyzed Friedel-Crafts polymerization for membrane gas separation, J. Membr. Sci. 644 (2022), 120115.
[11] L. Huang, W.J. Guo, H. Mondal, S. Schaefer, T.N. Tran, S.H. Fan, Y.F. Ding, H. Q. Lin, Effect of branch length on the structural and separation properties of hyperbranched poly(1,3-dioxolane), Macromolecules 55 (2022) 382–389.
[12] J. Wu, T.S. Chung, Supramolecular polymer network membranes with molecular-sieving nanocavities for efficient pre-combustion CO_2 capture, Small Methods 6 (2022), e2101288.
[13] M.A. El-Okazy, L. Liu, M.H. Abdellah, E. Goudeli, S.E. Kentish, Gas sorption and diffusion in perfluoro(butenyl vinyl ether) based perfluoropolymeric membranes, J. Membr. Sci. 644 (2022), 120095.
[14] L.M. Robeson, The upper bound revisited, J. Membr. Sci. 320 (2008) 390–400.
[15] B. Comesaña-Gándara, J. Chen, C.G. Bezzu, M. Carta, I. Rose, M.-C. Ferrari, E. Esposito, A. Fuoco, J.C. Jansen, N.B. McKeown, Redefining the Robeson upper bounds for CO_2/CH_4 and CO_2/N_2 separations using a series of ultrapermeable benzotriptycene-based polymers of intrinsic microporosity, Energy Environ. Sci. 12 (2019) 2733–2740.
[16] M. Liu, M.D. Nothling, P.A. Webley, Q. Fu, G.G. Qiao, Postcombustion carbon capture using thin-film composite membranes, Acc. Chem. Res. 52 (2019) 1905–1914.
[17] K. Xie, Q. Fu, G.G. Qiao, P.A. Webley, Recent progress on fabrication methods of polymeric thin film gas separation membranes for CO2 capture, J. Membr. Sci. 572 (2019) 38–60.
[18] T.C. Merkel, H.Q. Lin, X.T. Wei, R. Baker, Power plant post-combustion carbon dioxide capture: an opportunity for membranes, J. Membr. Sci. 359 (2010) 126–139.
[19] R.S. Bhavsar, T. Mitra, D.J. Adams, A.I. Cooper, P.M. Budd, Ultrahigh-permeance PIM-1 based thin film nanocomposite membranes on PAN supports for CO_2 separation, J. Membr. Sci. 564 (2018) 878–886.
[20] Y.F. Ji, M.C. Zhang, K.C. Guan, G.P. Liu, W.Q. Jin, J. Zhao, High-performance CO_2 capture through polymer-based ultrathin membranes, Adv. Funct. Mater. 29 (2019), 1900735.
[21] M. Liu, M.D. Nothling, P.A. Webley, J.Y. Jin, Q. Fu, G.G. Qiao, High-throughput CO_2 capture using PIM-1@MOF based thin film composite membranes, Chem. Eng. J. 396 (2020), 125328.
[22] C.S. Lee, M. Kang, K.C. Kim, J.H. Kim, In-situ formation of asymmetric thin-film, mixed-matrix membranes with ZIF-8 in dual-functional imidazole-based comb copolymer for high-performance CO_2 capture, J. Membr. Sci. 642 (2022), 119913.
[23] M. Liu, K. Xie, M.D. Nothling, P.A. Gurr, S.S.L. Tan, Q. Fu, P.A. Webley, G.G. Qiao, Ultrathin metal-organic framework nanosheets as a gutter layer for flexible composite gas separation membranes, ACS Nano 12 (2018) 11591–11599.
[24] I. Borisov, D. Bakhtin, J.M. Luque-Alled, A. Rybakova, V. Makarova, A.B. Foster, W.J. Harrison, V. Volkov, V. Polevaya, P. Gorgojo, E. Prestat, P.M. Budd, A. Volkov, Synergistic enhancement of gas selectivity in thin film composite membranes of PIM-1, J. Mater. Chem. 7 (2019) 6417–6430.
[25] Q. Fu, J. Kim, P.A. Gurr, J.M.P. Scofield, S.E. Kentish, G.G. Qiao, A novel cross-linked nano-coating for carbon dioxide capture, Energy Environ. Sci. 9 (2016) 434–440.
[26] J. Kim, Q. Fu, K. Xie, J.M.P. Scofield, S.E. Kentish, G.G. Qiao, CO_2 separation using surface-functionalized SiO_2 nanoparticles incorporated ultra-thin film composite mixed matrix membranes for post-combustion carbon capture, J. Membr. Sci. 515 (2016) 54–62.
[27] M. Guo, J. Qian, R. Xu, X. Ren, J. Zhong, M. Kanezashi, Boosting the CO_2 capture efficiency through aromatic bridged organosilica membranes, J. Membr. Sci. 643 (2022), 120018.
[28] D. Wang, Y. Ying, Y. Zheng, Y. Pu, Z. Yang, D. Zhao, Induced polymer crystallinity in mixed matrix membranes by metal-organic framework nanosheets for gas separation, J. Membr. Sci. Lett. 2 (2022), 100017.
[29] Z. Qiao, S. Zhao, M. Sheng, J. Wang, S. Wang, Z. Wang, C. Zhong, M.D. Guiver, Metal-induced ordered microporous polymers for fabricating large-area gas separation membranes, Nat. Mater. 18 (2019) 163–168.
[30] N.B. McKeown, P.M. Budd, Exploitation of intrinsic microporosity in polymer-based materials, Macromolecules 43 (2010) 5163–5176.
[31] A.B. Foster, M. Tamaddondar, J.M. Luque-Alled, W.J. Harrison, Z. Li, P. Gorgojo, P. M. Budd, Understanding the topology of the polymer of intrinsic microporosity PIM-1: cyclics, tadpoles, and network structures and their impact on membrane performance, Macromolecules 53 (2020) 569–583.
[32] A. Devarajan, E.D. Asuquo, M.Z. Ahmad, A.B. Foster, P.M. Budd, Influence of polymer topology on gas separation membrane performance of the polymer of intrinsic microporosity PIM-Py, ACS Appl. Polym. Mater. 3 (2021) 3485–3495.
[33] S. Aloraini, M. Mathias, J. Crone, K. Bryce, M. Yu, R.A. Kirk, M.Z. Ahmad, E. D. Asuquo, S. Rico-Martínez, A.V. Volkov, A.B. Foster, P.M. Budd, Crosslinking of branched PIM-1 and PIM-Py membranes for recovery of toluene from dimethyl sulfoxide by pervaporation, ACS Appl. Polym. Mater. 5 (2023) 1145–1158.
[34] A.B. Foster, J.L. Beal, M. Tamaddondar, J.M. Luque-Alled, B. Robertson, M. Mathias, P. Gorgojo, P.M. Budd, Importance of small loops within PIM-1 topology on gas separation selectivity in thin film composite membranes, J. Mater. Chem. 9 (2021) 21807–21823.
[35] K. Mizrahi Rodriguez, S. Lin, A.X. Wu, G. Han, J.J. Teesdale, C.M. Doherty, Z. P. Smith, Leveraging free volume manipulation to improve the membrane separation performance of amine-functionalized PIM-1, Angew Chem. Int. Ed. Engl. 60 (2021) 6593–6599.
[36] D. Jung, Z. Chen, S. Alayoglu, M.R. Mian, T.A. Goetjen, K.B. Idrees, K. O. Kirlikovali, T. Islamoglu, O.K. Farha, Postsynthetically modified polymers of intrinsic microporosity (PIMs) for capturing toxic gases, ACS Appl. Mater. Interfaces 13 (2021) 10409–10415.
[37] S. Xu, Y. Jin, R. Li, M. Shan, Y. Zhang, Amidoxime modified polymers of intrinsic microporosity/alginate composite hydrogel beads for efficient adsorption of cationic dyes from aqueous solution, J. Colloid Interface Sci. 607 (2022) 890–899.
[38] B. Satilmis, P.M. Budd, Base-catalysed hydrolysis of PIM-1: amide versus carboxylate formation, RSC Adv. 4 (2014) 52189–52198.
[39] J.W. Jeon, D.G. Kim, E.H. Sohn, Y. Yoo, Y.S. Kim, B.G. Kim, J.C. Lee, Highly carboxylate-functionalized polymers of intrinsic microporosity for CO_2-selective polymer membranes, Macromolecules 50 (2017) 8019–8027.
[40] K. Mizrahi Rodriguez, A.X. Wu, Q. Qian, G. Han, S. Lin, F.M. Benedetti, H. Lee, W. S. Chi, C.M. Doherty, Z.P. Smith, Facile and time-efficient carboxylic acid functionalization of PIM-1: effect on molecular packing and gas separation performance, Macromolecules 53 (2020) 6220–6234.
[41] W.Y. Han, C.L. Zhang, M. Zhao, F. Yang, Y. Yang, Y.X. Weng, Post-modification of PIM-1 and simultaneously in situ synthesis of porous polymer networks into PIM-1 matrix to enhance CO_2 separation performance, J. Membr. Sci. 636 (2021), 119544.
[42] B. Santoso, P. Yanaranop, H. Kang, I.K.H. Leung, J. Jin, A critical update on the synthesis of carboxylated polymers of intrinsic microporosity (C-PIMs), Macromolecules 50 (2017) 3043–3050.
[43] N.Y. Du, G.P. Robertson, J.S. Song, I. Pinnau, M.D. Guiver, High-performance carboxylated polymers of intrinsic microporosity (PIMs) with tunable gas transport properties, Macromolecules 42 (2009) 6038–6043.
[44] W.F. Yong, P. Salehian, L. Zhang, T.-S. Chung, Effects of hydrolyzed PIM-1 in polyimide-based membranes on C2–C4 alcohols dehydration via pervaporation, J. Membr. Sci. 523 (2017) 430–438.
[45] K.S. Liao, J.Y. Lai, T.S. Chung, Metal ion modified PIM-1 and its application for propylene/propane separation, J. Membr. Sci. 515 (2016) 36–44.
[46] H.Y. Zhao, Q. Xie, X.L. Ding, J.M. Chen, M.M. Hua, X.Y. Tan, Y.Z. Zhang, High performance post-modified polymers of intrinsic microporosity (PIM-1) membranes based on multivalent metal ions for gas separation, J. Membr. Sci. 514 (2016) 305–312.
[47] Y. Pan, X. Zhai, J. Yin, T. Zhang, L. Ma, Y. Zhou, Y. Zhang, J. Meng, Hierarchical porous and zinc-ion-crosslinked PIM-1 nanocomposite as a CO_2 cycloaddition catalyst with high efficiency, ChemSusChem 12 (2019) 2231–2239.
[48] R. Wu, Y.H. Li, A.S. Huang, Synthesis of high-performance Co-based ZIF-67 membrane for H_2 separation by using cobalt ions chelated PIM-1 as interface layer, J. Membr. Sci. 620 (2021), 118841.
[49] W.H. Wu, P. Thomas, P. Hume, J. Jin, Effective conversion of amide to carboxylic acid on polymers of intrinsic microporosity (PIM-1) with nitrous acid, Membranes 8 (2018) 20.
[50] H. Ling, O.T. Qazvini, S.G. Telfer, J. Jin, Effective enhancement of selectivities and capacities for CO_2 over CH_4 and N_2 of polymers of intrinsic microporosity via postsynthesis metalation, J. Polym. Sci. 58 (2020) 2619–2624.
[51] X. Weng, J.E. Baez, M. Khiterer, M.Y. Hoe, Z. Bao, K.J. Shea, Chiral polymers of intrinsic microporosity: selective membrane permeation of enantiomers, Angew Chem. Int. Ed. Engl. 54 (2015) 11214–11218.
[52] N. Du, J. Song, G.P. Robertson, I. Pinnau, M.D. Guiver, Linear high molecular weight ladder polymer via fast polycondensation of 5,5′,6,6′-Tetrahydroxy-3,3,3′,3′-tetramethylspirobisindane with 1,4-Dicyanotetrafluorobenzene, macromol, Rapid Commun. 29 (2008) 783–788.

[53] M. Yu, A.B. Foster, C.A. Scholes, S.E. Kentish, P.M. Budd, Methanol vapor retards aging of PIM-1 thin film composite membranes in storage, ACS Macro Lett. 12 (2023) 113–117.
[54] M.A. El-Okazy, L. Liu, Y.C. Zhang, S.E. Kentish, The impact of water, BTEX compounds and ethylene glycol on the performance of perfluoro(butenyl vinyl ether) based membranes for CO_2 capture from natural gas, J. Membr. Sci. 654 (2022), 120557.
[55] W.F. Yong, F.Y. Li, T.S. Chung, Y.W. Tong, Molecular interaction, gas transport properties and plasticization behavior of cPIM-1/Torlon blend membranes, J. Membr. Sci. 462 (2014) 119–130.
[56] B. Satilmis, Amidoxime modified polymers of intrinsic microporosity (PIM-1); A versatile adsorbent for efficient removal of charged dyes; equilibrium, kinetic and thermodynamic studies, J. Polym. Environ. 28 (2020) 995–1009.
[57] A.K. Sekizkardes, S. Budhathoki, L. Zhu, V. Kusuma, Z. Tong, J.S. McNally, J. A. Steckel, S. Yi, D. Hopkinson, Molecular design and fabrication of PIM-1/polyphosphazene blend membranes with high performance for CO_2/N_2 separation, J. Membr. Sci. 640 (2021), 119764.
[58] X. Mei Wu, Q. Gen Zhang, P. Ju Lin, Y. Qu, A. Mei Zhu, Q. Lin Liu, Towards enhanced CO_2 selectivity of the PIM-1 membrane by blending with polyethylene glycol, J. Membr. Sci. 493 (2015) 147–155.
[59] Q. Song, S. Cao, R.H. Pritchard, B. Ghalei, S.A. Al-Muhtaseb, E.M. Terentjev, A. K. Cheetham, E. Sivaniah, Controlled thermal oxidative crosslinking of polymers of intrinsic microporosity towards tunable molecular sieve membranes, Nat. Commun. 5 (2014) 4813.
[60] M. Tamaddondar, A.B. Foster, M. Carta, P. Gorgojo, N.B. McKeown, P.M. Budd, Mitigation of physical aging with mixed matrix membranes based on cross-linked PIM-1 fillers and PIM-1, ACS Appl. Mater. Interfaces 12 (2020) 46756–46766.
[61] R.R. Tiwari, Z.P. Smith, H. Lin, B.D. Freeman, D.R. Paul, Gas permeation in thin films of “high free-volume” glassy perfluoropolymers: Part I, Phys. aging, Polym. 55 (2014) 5788–5800.
[62] P.B. Bernardo, F. Tasselli, G. Clarizia, C.R.M.-A. Mason, P.M.L. Budd, M.K. V. Pilnáček, O.K.F. Friess, Yu P. Yampolskii, V. Shantarovich, J.C. Jansen, Effect of physical aging on the gas transport and sorption in PIM-1 membranes, Polymer 113 (2017) 283–294.
[63] F. Almansour, M. Alberto, A.B. Foster, S. Mohsenpour, P.M. Budd, P. Gorgojo, Thin film nanocomposite membranes of superglassy PIM-1 and amine-functionalised 2D fillers for gas separation, J. Mater. Chem. 10 (2022) 23341–23351.
[64] T.H. Lee, M.G. Shin, J.G. Jung, E.H. Suh, J.G. Oh, J.H. Kang, B.S. Ghanem, J. Jang, J.H. Lee, I. Pinnau, H.B. Park, Facile suppression of intensified plasticization in glassy polymer thin films towards scalable composite membranes for propylene/propane separation, J. Membr. Sci. 645 (2022), 120215.
[65] M. Cook, P.R.J. Gaffney, L.G. Peeva, A.G. Livingston, Roll-to-roll dip coating of three different PIMs for Organic Solvent Nanofiltration, J. Membr. Sci. 558 (2018) 52–63.
[66] E. Chernova, D. Petukhov, O. Boytsova, A. Alentiev, P. Budd, Y. Yampolskii, A. Eliseev, Enhanced gas separation factors of microporous polymer constrained in the channels of anodic alumina membranes, Sci. Rep. 6 (2016), 31183.
[67] R. Swaidan, B. Ghanem, E. Litwiller, I. Pinnau, Physical aging, plasticization and their effects on gas permeation in "rigid" polymers of intrinsic microporosity, Macromolecules 48 (2015) 6553–6561.
[68] M. Wessling, M.L. Lopez, H. Strathmann, Accelerated plasticization of thin-film composite membranes used in gas separation, Sep. Purif. Technol. 24 (2001) 223–233.
[69] W. Ogieglo, B. Ghanem, X. Ma, M. Wessling, I. Pinnau, High-pressure CO_2 sorption in polymers of intrinsic microporosity under ultrathin film confinement, ACS Appl. Mater. Interfaces 10 (2018) 11369–11376.
[70] R.R. Tiwari, J. Jin, B.D. Freeman, D.R. Paul, Physical aging, CO_2 sorption and plasticization in thin films of polymer with intrinsic microporosity (PIM-1), J. Membr. Sci. 537 (2017) 362–371.
[71] P. Li, T.S. Chung, D.R. Paul, Temperature dependence of gas sorption and permeation in PIM-1, J. Membr. Sci. 450 (2014) 380–388.
[72] Y. Ren, B. Chong, W. Xu, Z. Zhang, L. Liu, Y. Wu, Y. Liu, H. Jiang, X. Liang, H. Wu, H. Zhang, B. Ye, C. Zhong, G. He, Z. Jiang, Coordination-driven structure reconstruction in polymer of intrinsic microporosity membranes for efficient propylene/propane separation, Innovation 3 (2022), 100334.
[73] A.J. Hill, S.J. Pas, T.J. Bastow, M.I. Burgar, K. Nagai, L.G. Toy, B.D. Freeman, Influence of methanol conditioning and physical aging on carbon spin-lattice relaxation times of poly(1-trimethylsilyl-1-propyne), J. Membr. Sci. 243 (2004) 37–44.
[74] S. Harms, K. Ratzke, F. Faupel, N. Chaukura, P.M. Budd, W. Egger, L. Ravelli, Aging and free volume in a polymer of intrinsic microporosity (PIM-1), J. Adhes. 88 (2012) 608–619.
[75] F. Almansour, M. Alberto, R.S. Bhavsar, X.L. Fan, P.M. Budd, P. Gorgojo, Recovery of free volume in PIM-1 membranes through alcohol vapor treatment, Front. Chem. Sci. Eng. 15 (2021) 872–881.